

Directional light emission from WS₂ monolayer driven by self-hybridized van der Waals nanoresonator

Shiyu Shen,¹ Haojie Zhou,¹ Peng Xie,¹ Qi Ding,¹ Ling Yue,¹ Jinglei Du,¹ Hong Zhang,^{1,2} and Wei Wang^{1,*}

¹College of Physics, Sichuan University, Chengdu 610064, China

²Key Laboratory of High Energy Density Physics and Technology of Ministry of Education, Sichuan University, Chengdu 610065, China

 (Received 25 November 2023; revised 12 March 2024; accepted 13 March 2024; published 2 April 2024)

Bulk transition-metal dichalcogenides (TMDs) materials are becoming attractive candidates for the study of light-matter interactions and manipulation of light emission due to its surprisingly high refractive index in visible to infrared range. Here, we propose a nanoresonator composed of bulk tungsten disulfide (WS₂) as an all-dielectric nanoantenna, demonstrating its capability in controlling the emission of light. We demonstrate that the WS₂ nanowire can efficiently control the emission directionality of an adjacent quantum emitter via multimode interference and self-hybridization. The influence of oscillator strength of the intrinsic excitonic mode on the directional emission property is investigated. We reveal that exciton-Mie self-hybridization can effectively modulate the emission directionality leading to a dramatic suppression of directional emission at the excitonic resonances. We also demonstrate that the light emission from monolayer WS₂ can be controlled by adjusting the radius of the nanowire, achieving unidirectional and directional radiation at different nanowire radius, which is attributed to the mutual interference between different optical modes. The proposed system is expected to offer a promising route for potential applications in ultracompact and multiplexed integrated photonic devices.

DOI: [10.1103/PhysRevB.109.155405](https://doi.org/10.1103/PhysRevB.109.155405)

I. INTRODUCTION

Manipulating light at the nanoscale is the basis of a wide range of applications including the integration of photonic devices and optical chips [1–3]. In recent years, effective control of light, in particular the manipulation of radiation directionality has become a very important subject and has been widely studied. This is of great importance for improving the efficiency of optoelectronic systems [4], as quantum emitters, two-dimensional semiconductors [5], quantum dots [6,7], and color centers [8] are becoming promising platforms for next-generation integrated photonic devices, such as nanoscale light sources [9–12]. Effective control of light emission properties from these quantum emitters has important applications, including solid-state lighting and displays [13,14].

Metal nanoantennas, including Yagi-Uda antenna [15], dimers [16,17], v-shaped antennas [18], etc., can excite surface plasmon modes to capture and concentrate light at subwavelength scales to achieve large-field localization, which is one of the most promising solutions for controlling the direction of optical radiation. However, conventional plasmonic nanoantennas suffer from intrinsic Ohmic losses [19,20], which are incompatible with most semiconductor device-processing technologies. This strongly affects their overall performance and limits their potential applications.

High-refractive-index dielectric materials are becoming complementary platforms for the manipulation of radiation directionality [21–25]. Compared to metallic nanostructures,

cost-effective dielectric materials can be easily handled by using mature semiconductor fabrication techniques with high compatibility [14,26–28]. Resonances in high refractive-index dielectrics are excited with low energy losses even in the optical and near-infrared (NIR) regions, owing to the absence of free-electron absorption. Furthermore, magnetic resonances can be excited, originating from the rotation of the displacement current [29,30]. The mutual interference between the magnetic and electrical modes leads to a directional regulation of light, like Kerker effect [31–33]. Studies of the Kerker effect have shown that resonant multipole excitation of nanostructures can be used to direct the flow of light very effectively. The far-field scattering of each multipole has a unique angular distribution and phase symmetry. When two or more multipoles are simultaneously excited, a strong interference effect can be observed and used to direct the scattered light. In addition, interference between different modes can also lead to unidirectional and bidirectional radiation, etc. [34,35].

Recent exploration has extended to multilayer or bulk transition-metal dichalcogenides (TMDs) as alternative platforms for manipulating emission of light [36–39]. Dielectric nanostructures based on bulk TMD materials, characterized by very large in-plane refractive indices higher than the best high-index semiconductor materials such as silicon or germanium, can excite multiple Mie resonances, and therefore can function as resonant nanoresonators. Importantly, such TMD-based nanoresonators possess intrinsic excitons, which can directly couple to the Mie resonances supported by the nanoresonator itself, leading to self-hybridized exciton polaritons [37,39]. So far, there has been a lack of in-depth discussions on the use of bulk TMD materials as optical nanoantennas for controllable directionality. Moreover, bulk

*w.wang@scu.edu.cn

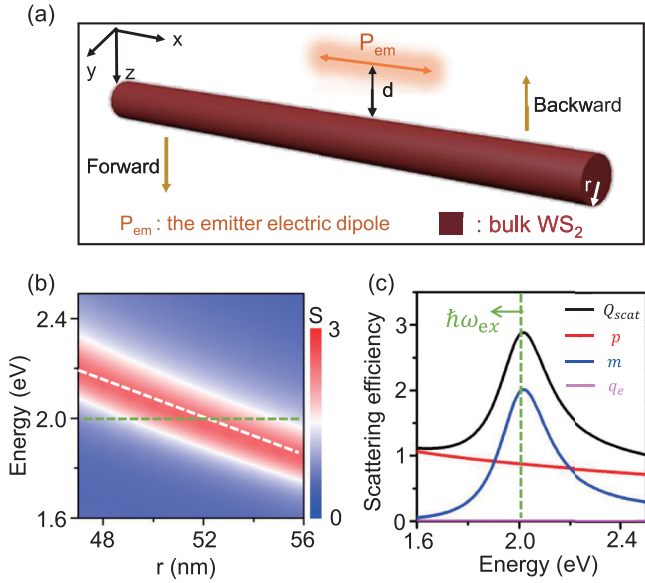


FIG. 1. (a) Schematic of the bulk WS_2 nanowire under excitation by the electric dipole source. (b) Scattering spectra (in color scale) with different radius r . (c) Scattering efficiency and multipolar contributions (electric dipole p , magnetic dipole m and electric quadrupole q_e) of the nanowire with $f_0 = 0$ at zero detuning.

TMDs exhibit self-hybridization coupling between Mie resonance and exciton mode [40,41], suggesting potential for exploring directed radiation at specific wavelengths through interference between different modes.

Here, we propose a nanowire composed of bulk tungsten disulfide (WS_2) as a dielectric nanoantenna to examine its capability in controlling the emission of light. We demonstrate that the nanowire can efficiently control the emission directionality of an adjacent quantum emitter via multimode interactions and self-hybridizations. The influence of oscillator strength of the intrinsic excitonic mode on the directional emission property is investigated, revealing the fact that exciton-Mie self-hybridization can effectively modulate the emission directionality, leading to a dramatic suppression of directional emission at the excitonic resonances. We also demonstrate that the light emission from monolayer WS_2 can be controlled by adjusting the radius of the nanowire, achieving unidirectional and directional radiation at different nanowire radius. The phase diagrams reveal the underlying physical mechanism: modulation on light emission originates from the mutual interference among magnetic dipole, electric dipole, and quadrupole mode.

II. RESULTS AND DISCUSSIONS

A. Strong self-hybridization in the bulk WS_2 nanowire

The proposed nanoresonator is composed of a bulk WS_2 nanowire with a radius r , as shown in Fig. 1(a). We selected an electric dipole emitter 1 nm away from the nanowire ($d = 1$ nm) as the excitation source, and the excitation direction was parallel to the nanowire. The localized dipole models the exciton emission from the monolayer TMD. In addition, the forward scattering and backward scattering of the nanowire to

the dipole source are marked. In this work, we theoretically investigated optical response of the nanowire under dipole-source excitation, including the self-hybridization effect of the nanowire, the radiation characteristics from the nanowire to the dipole emitter, including the forward and backward scattering efficiency, and the ratio of the forward and backward radiation.

To investigate the self-hybridization effect of the bulk WS_2 nanowire under the electric dipole excitation, we calculated the scattering efficiency of the nanowire using the modified Mie theory [42]

$$Q_{\text{scat}}^{\text{dipole}} = P_{\text{scat}}/P_{\text{inc}} = \sum_{n=-\infty}^{\infty} |b_n|^2 |H_n^{(1)}[k_0(R+d)]|^2. \quad (1)$$

Here, P_{scat} and P_{inc} denote the scattered and incident powers as a function of the scattered and incident electric fields. b_n is the conventional Mie coefficient. $H_n^{(1)}$ is the first-order Hankel function. k_0 , R , d are the vacuum wave number, radius of the WS_2 nanowire, and the distance from dipole to nanowire, respectively. For the calculation of scattering efficiency with the WS_2 nanowire, a complex dielectric function as a Lorentz oscillator is considered [43]:

$$\epsilon = \epsilon_0 + f_0 \frac{\omega_{ex}^2}{\omega_{ex}^2 - \omega^2 - i\gamma_{ex}\omega}. \quad (2)$$

Here, $\epsilon_0 = 20$ is background permittivity, f_0 is the oscillator strength, ω_{ex} is resonance energy of exciton, and γ_{ex} is the exciton full width.

We first calculated the scattering efficiency of the nanowire as a “pure” high-refractive-index Mie resonator. For this purpose, the intrinsic exciton transition is “switched off” by setting $f_0 = 0$. Figure 1(b) gives the spectra of the scattering efficiency (in color scale) as a function of the radius r of the nanowire. A prominent Mie resonance is visible with two distinct aspects: (i) The resonance red shifts linearly from 2.2 eV to 1.75 eV as the radius increases from $r = 47$ nm to $r = 56$ nm, as marked by the white dashed line, and importantly (ii) the Mie resonance shifts across the transition energy of the A exciton (dashed green line) of the bulk WS_2 at $\hbar\omega_{ex} = 2$ eV (620 nm).

To fully understand the optical response of the nanowire, we calculated the scattering efficiency and the multipolar contributions for the radius of $r = 51$ nm, as shown in Fig. 1(c). Note that the radius of the nanowire was chosen such that the Mie resonance can still cover the spectral region of interest to facilitate its interaction with the excitons ($\hbar\omega_{ex}$). We can clearly see that the magnetic dipole m dominates in the scattering power, particularly at the scattering peak. The results are helpful to understand the far-field characteristics of the Mie resonance and its hybridized interaction with excitons, which will be discussed in the later section.

To further study of the self-hybridization effect in the bulk WS_2 nanowire, we “switched on” the excitonic transition by applying a nonzero value of f_0 . Figure 2(a) plots the scattering spectra (in color scale) as a function of the nanowire radius r ranging from 47 nm to 56 nm with $f_0 = 0.2$. Two distinct bending branches appear in the spectrum with typical anticrossing behavior. This indicates that coupling between the magnetic Mie resonance and the excitons is realized,

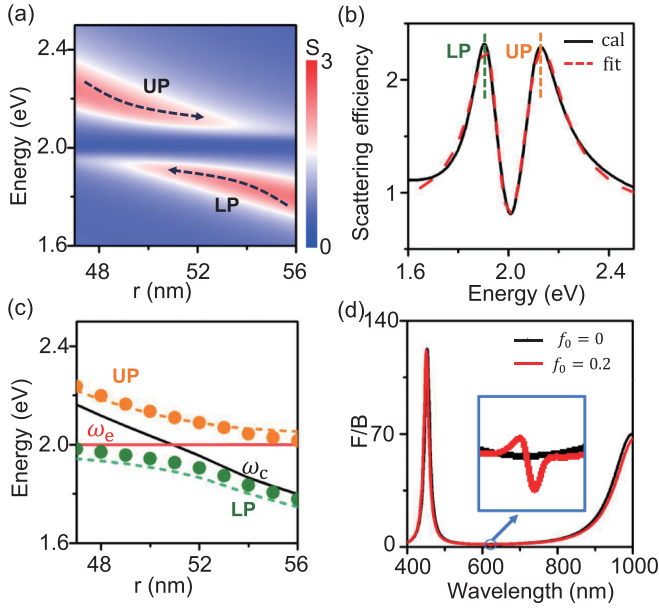


FIG. 2. (a) Calculated scattering spectra (in color scale) of the self-hybridized system as a function of nanowire radius r . (b) Calculated (solid black) and fitted (dashed red) scattering spectrum of the hybrid system at zero detuning ($r = 51$ nm). (c) The calculated (dashed curves) and fitted (solid circle) dispersion relation of the hybrid system. (d) F/B ratio with different f_0 of the dielectric function for the bulk WS₂ nanowire. The inset gives the zoomed-in picture at resonance for the structure.

resulting in the emergence of high-energy polariton (UP) and low-energy polariton (LP). The coupling properties, such as spectral width, energetics, coupling strength, and more optical details of the newly formed states, can be quantitatively evaluated by fitting the calculated spectra to a Fano-like line shape. The scattering spectrum $S(\omega) = |s(\omega)|^2$ can be expressed as [44]

$$s(\omega) = a_b + \sum_j^N \frac{b_j \gamma_j e^{i\phi_j}}{\omega - \omega_j + i\gamma_j}. \quad (3)$$

Here, a_b , b_j , γ_j , ϕ_j are the background amplitude, amplitude, damping rate, and phase of the spectra, respectively. ω_j and $2\gamma_j$ are the resonance and the scattering spectrum full width at half maximum (FWHM) of the hybrid states. Figure 2(b) gives the scattering efficiency spectra with the radius $r = 51$ nm at zero detuning (the exciton is exactly in resonance with the magnetic Mie mode). It can be seen that the calculated spectrum (solid black line) can almost perfectly overlap with the Fano-like fitted spectrum (dashed red line), which indicates that the inhomogeneous broadening of the hybrid states has

little effect or small contribution on the scattering spectrum. Based on this, we use the Fano-like line shape to fit the calculated scattering spectrum as a function of the nanowire radius r , as shown by solid circles in Fig. 2(c).

To give a deep insight of the coupling between the magnetic Mie resonance and the excitons, we quantitatively calculated the coupling strength by employing a 2×2 Hamiltonian matrix [45]

$$H = \hbar \begin{pmatrix} \tilde{\omega}_{\text{ex}} & g \\ g & \tilde{\omega}_{\text{M}} \end{pmatrix}. \quad (4)$$

Here, $\tilde{\omega}_{\text{ex}} = \omega_{\text{ex}} - i\gamma_{\text{ex}}$, $\tilde{\omega}_{\text{M}} = \omega_{\text{M}} - i\gamma_{\text{M}}$ represent the complex resonance frequencies of the WS₂ excitons and the magnetic Mie resonance, respectively. ω_{ex} and ω_{M} represent the eigenenergies of these two modes, respectively, as shown by the solid lines in Fig. 2(c). $2\gamma_{\text{ex}}$ and $2\gamma_{\text{M}}$ are FWHM. g is used to describe the coupling strength. Diagonalizing Eq. (4), the dispersions and damping rates of the polariton modes are given by the real and imaginary parts of the complex eigenvalues:

$$E_{\pm} = \hbar \tilde{\omega}_{\pm} = \hbar \left(\frac{\tilde{\omega}_{\text{ex}} + \tilde{\omega}_{\text{M}}}{2} \right) \pm \hbar \sqrt{g^2 + \left(\frac{\tilde{\omega}_{\text{M}} - \tilde{\omega}_{\text{ex}}}{2} \right)^2}. \quad (5)$$

The coupling strength can be given by Rabi splitting (Ω_R) as

$$g = \frac{1}{2} \sqrt{\Omega_R^2 + (\gamma_{\text{ex}} - \gamma_{\text{M}})^2}. \quad (6)$$

In order to determine that the coupled system is in the strong-coupling regime, the Rabi-splitting energy should exceed the sum of the spectral widths of the two hybrid polariton bands and satisfy the following formula [46]:

$$g > \sqrt{(\gamma_{\text{ex}}^2 + \gamma_{\text{M}}^2)/2}. \quad (7)$$

We solved Eq. (4) and very nicely reproduced the dispersion of the hybrid modes, as shown by the dashed lines in Fig. 2(c), which overlapped well with the fitted results with an optimized coupling energy $\hbar\Omega_R = 120$ meV. The corresponding spectral width of the magnetic Mie resonance and the exciton modes are $\hbar\Gamma_{\text{M}} = 2\hbar\gamma_{\text{M}} = 210$ meV, $\hbar\Gamma_{\text{ex}} = 2\hbar\gamma_{\text{ex}} = 50$ meV, respectively. In this case, the strong coupling condition [Eq. (7)] is satisfied.

B. Directional emission from the dipole source mediated by the nanowire

In order to quantify the directionality and investigate the radiation characteristics of the nanowire under strong coupling, we calculated the ratio of the forward (F) and backward (B) radiation from the WS₂ nanowire to the electric dipole source using the following equation [42]:

$$I_{\text{ff}}(\theta) = \frac{\omega^2 \mu_0^2 I^2}{8\pi} \left| \sum_{n=-\infty}^{\infty} (-i)^n \{ J_n[k_0(R+d)] - b_n H_n^{(1)}[k_0(R+d)] \} e^{in\theta} \right|^2. \quad (8)$$

The ratio of F/B can be described as

$$F/B = \int_{\theta=108.2^\circ}^{\theta=251.8^\circ} I_{\text{ff}}(\theta) d\theta / \int_{\theta=326.5^\circ}^{\theta=33.5^\circ} I_{\text{ff}}(\theta) d\theta. \quad (9)$$

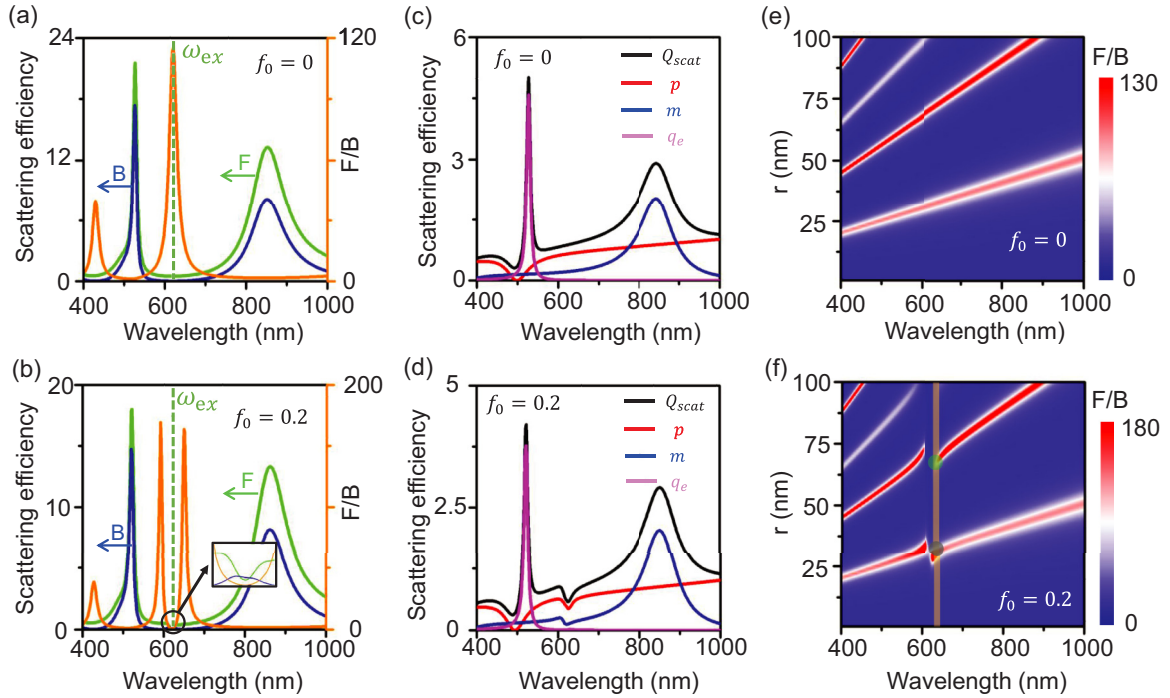


FIG. 3. Forward and backward scattering efficiency and F/B ratio for $r = 70$ nm with $f_0 = 0$ (a) and $f_0 = 0.2$ (b). Scattering efficiency and multipolar contributions for $r = 70$ nm with $f_0 = 0$ (c) and $f_0 = 0.2$ (d). F/B ratio (in color scale) of the bulk WS_2 nanowire to the dipole source with $f_0 = 0$ (e) and $f_0 = 0.2$ (f). The vertical shaded area corresponds to the emission band of the monolayer WS_2 , and the solid circles represent the maximum F/B ratio corresponding to the radius of the bulk WS_2 nanowire.

Here, μ_0 is the magnetic permeability of vacuum, I is the current of the line source, J_n is the Bessel function of the first kind, and θ is the emission angle. The forward and backward monitors with numerical apertures of 0.95 and 0.55 were selected. We calculated the ratio of F/B with $f_0 = 0$ and $f_0 = 0.2$ of the dielectric function for bulk WS_2 at zero detuning, respectively, by solving Eq. (8) and Eq. (9), as shown in Fig. 2(d). Apparently, the two lines are perfectly overlapped indicating that the strong exciton-Mie coupling does not affect the F/B ratio from the nanowire to the electric dipole source. Note that the inset gives the zoomed-in picture at exciton resonance. The presence of excitons causes a small peak in the F/B spectrum at $\lambda = 620$ nm with $f_0 = 0.2$, which has little effect on the F/B spectrum.

To explore the influence of the oscillator strength (f_0) on the ratio of F/B from the nanowire to the dipole source and the underlying physical mechanism, we calculated the forward and backward scattering efficiency and F/B ratio for different f_0 with $r = 70$ nm by solving Eq. (9). Figure 3(a) illustrates the forward (green curve) and backward (blue curve) scattering efficiency and F/B ratio (orange curve) with $f_0 = 0$. Three main features can clearly be seen: (i) Two Mie resonances are excited by the dipole source in this wavelength band due to the high-refractive-index of the nanowire, and the resonance positions of the forward and backward scattering spectra are essentially the same. (ii) The peaks of the F/B ratio spectra occur between the different Mie resonances, primarily originating from the interference between these two resonances. In addition, the maximum value occurs exactly at the position of the exciton resonance (dashed green line). (iii) The F/B ratio is as high as 120 at $\lambda = 620$ nm, which implies that the

nanowire can effectively manipulate the light from the dipole source and modulate the forward radiation at this wavelength.

For the case of $f_0 = 0.2$, the forward and backward scattering spectra are similar to those of $f_0 = 0$, as evidenced by two distinct Mie resonances in Fig. 3(b). Furthermore, compared to the scattering spectra of $f_0 = 0$, the bulk WS_2 nanowire can excite not only Mie resonances, but also an exciton mode, as shown in the inset of Fig. 3(b), which gives the zoom-in picture at resonance. More importantly, we find that the presence of the exciton mode results in a suppressed F/B ratio at $\lambda = 620$ nm, with two distinct peaks appearing on the left and right sides of the position. The F/B ratio is up to 178, which is higher than that for the case of $f_0 = 0$. This implies a superior forward modulation from the nanowire to the dipole source.

In order to reveal the mechanism behind the suppression of the F/B ratio at $\lambda = 620$ nm and to fully understand the far-field scattering spectral response, we quantitatively characterized the excitation of the different electromagnetic modes that may lead to the Mie resonance using multipole expansion methods with different f_0 , as shown in Fig. 3(c) and Fig. 3(d). This analysis contributes to the understanding of the far-field spectral properties of the Mie resonance and its effect on the F/B ratio. Three main features can clearly be seen: (i) The two Mie resonances in the scattering spectrum are dominated by the magnetic dipole m and the electric quadrupole q_e with $f_0 = 0$, respectively, which interact with each other thus leading to a high F/B ratio at $\lambda = 620$ nm; (ii) The electric dipole (p) mode shows a much reduced value of the scattering power at the Mie resonance dominated by the electric quadrupole is greatly reduced; (iii) In contrast to $f_0 = 0$, the scattering

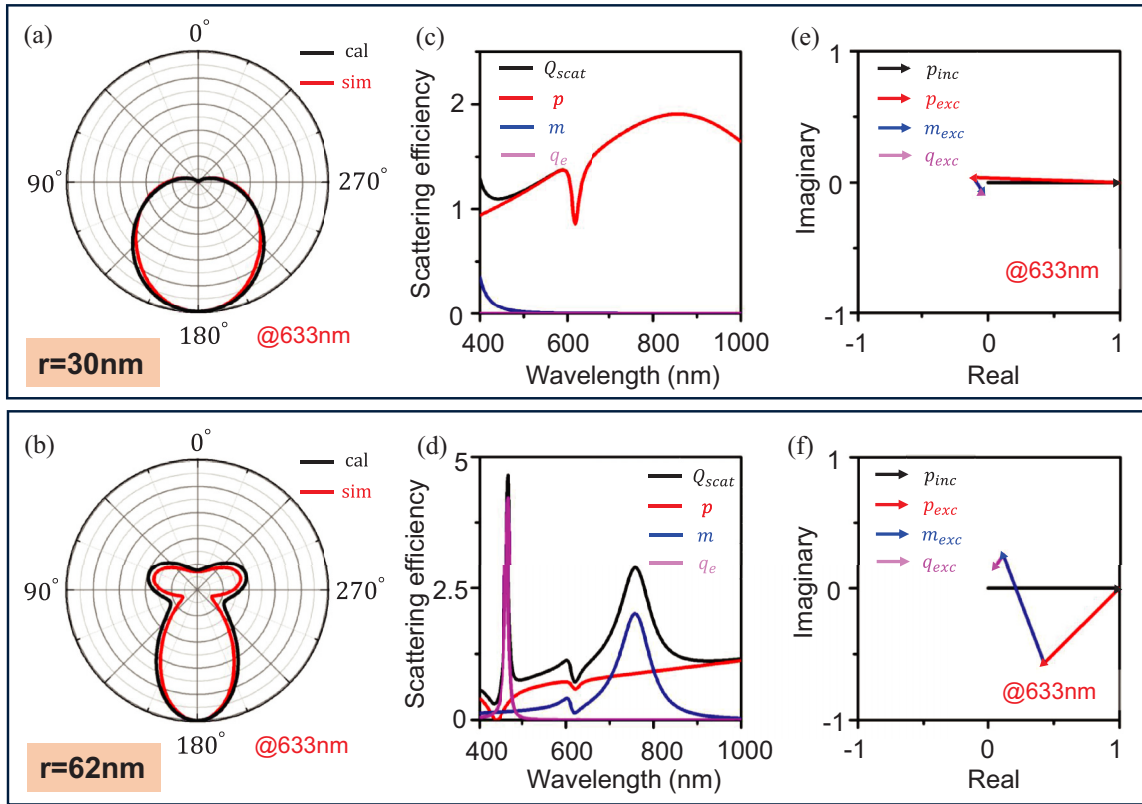


FIG. 4. The radiation pattern for dipole excitation of the bulk WS₂ nanowire with $r = 30$ nm (a) and $r = 62$ nm (b) at $\lambda = 633$ nm. Scattering efficiency and multipolar contributions of the self-hybridized system for $r = 30$ nm (c) and $r = 62$ nm (d). Phasor representations of the electric fields at a position in the backward emission direction for $r = 30$ nm (e) and $r = 62$ nm (f).

spectrum contains not only Mie resonances dominated by magnetic dipoles and electric quadrupoles, but also exciton modes contributing mainly to electric and magnetic dipole with $f_0 = 0.2$. As a result, the exciton mode interacts with each of the two Mie resonances, resulting in higher F/B ratio at the left and right sides of the exciton position, respectively, while the F/B ratio is suppressed at that position in comparison with $f_0 = 0$.

To better understand the effect of exciton mode on the F/B ratio, we further calculated the F/B ratio at $f_0 = 0$ and $f_0 = 0.2$ as a function of the nanowire radius r , as shown in Fig. 3(e) and Fig. 3(f). We can clearly see that the peak of the F/B ratio shifts almost linearly to red as the nanowire becomes larger (increasing radius r). The number of the bands gradually increase for both $f_0 = 0$ and $f_0 = 0.2$. It is well known that the resonance position can be readily tuned by controlling the geometry parameters of the system. More Mie resonances are excited as the nanowire radius increases. Each band can be identified with a unique directionality mechanism involving different multipolar Mie resonances. For the case of $f_0 = 0.2$, there are two distinct bands of the F/B spectrum around $\lambda = 620$ nm (the exciton position) that exhibit anticrossing behavior, which means there is no emission directionality at the exciton position. In addition, compared with Fig. 3(e), the interaction between the exciton mode and the Mie resonances leads to a significant increase of the F/B ratio.

On the other hand, the dipole source is used to model the exciton emission from the monolayer TMD. The poor

emission directionality and the low quantum efficiency of monolayer TMD have limited their practical applications. Therefore, it is important to select the suitable structural parameters to achieve the desired emission directionality. The orange shaded section in Fig. 3(f) shows the emission wavelength range of monolayer WS₂, and its overlap with the F/B band shows that the nanowire has excellent forward modulation of monolayer WS₂ emission. Also, we find that the F/B ratio in the orange region are the largest, 175 and 178 [as shown by the solid black and green circle in Fig. 3(f)], with $r = 30$ nm and $r = 62$ nm, respectively. This implies that nanowires at these two parameters have the best forward modulation of monolayer WS₂ emission, corresponding to two different emission modulation mechanisms, which will be discussed in detail in a later section.

C. Highly unidirectional/directional emission from WS₂ monolayer

To further study the nanowire-mediated directional emission from WS₂ monolayer, we calculated the far-field radiation pattern in the y - z direction at the emission band of WS₂ monolayer ($\lambda = 633$ nm) for the above-mentioned two cases ($r = 30$ nm, $r = 62$ nm), as shown in Figs. 4(a) and 4(b), respectively.

For the case of $r = 30$ nm, the far-field radiation pattern [Fig. 4(a)] exhibits forward unidirectional radiation with a single lobe (solid black line) oriented along the z direction,

corresponding to the high F/B ratio of 175 [black dot in Fig. 3(f)]. This matches very well with the simulated result (solid red line). Note that the length of the nanowire needs to be set long enough during the simulation to ensure the accuracy of the results.

To explore the nature of the higher F/B ratio and explain the physical mechanism of unidirectional radiation, we further calculated the scattering spectra of the nanowire with $r = 30$ nm and quantitatively characterized the multipole properties by means of the multipole expansion method, as shown in Fig. 4(c). A corresponding phasor representation [Fig. 4(e)] is also calculated to clearly show the relative magnitudes and phases of the multipoles. As can be seen in Fig. 4(c), the scattering efficiency Q_{scat} is dominated by the electric dipole mode p , while the contribution of the magnetic dipole m and electric quadrupole q_e are negligible. With the help of the phasor representation in Fig. 4(e), the underlying mechanism for unidirectional emission can be well explained by first Kerker effect: the strong dipolar emission (solid red arrow), with amplitude as large as that of the incident dipole source (solid black arrow), is out of phase with respect to the incident field of the reversed dipole radiation. The destructive interference of the scattered fields from the excited electric dipole resonance of the nanowire with those of the dipole emitter leads to the forward unidirectional radiation with a complete suppression of backward emission. In this case, the m and q_e components have very little contribution to the unidirectional radiation due to their weak scattering strength [blue and purple curves in Fig. 4(c)], corresponding to negligible amplitudes at the WS₂ emission band ($\lambda = 633$ nm) in the phasor representation diagram [blue and purple arrows in Fig. 4(e)].

For the case of $r = 62$ nm, the dipole source at WS₂ emission band radiates with different features compared to the case of $r = 30$ nm, as shown in Fig. 4(b). The emission pattern clearly shows a narrowed lobe around 180°, corresponding to a strong forward radiation with improved directionality. In particular, a small backward emission occurs with two tiny side lobes around 85° and 265°, indicating an imperfect unidirectional emission.

To give a deep insight into the directional emission, we also performed multipole decomposition and phasor plots for each component, as shown in Figs. 4(d) and 4(f), respectively. Obviously, at the two sides of WS₂ emission band, the electric dipole (red) and magnetic dipole (blue) components dominate in the scattering spectrum [Fig. 4(d)]. In this sense, the underlying mechanism of the modulated directionality is distinctly

different from that for the case of $r = 30$ nm: The interference between the nanowire-mediated electric dipole (red arrow) and magnetic dipole (blue arrow) components cancels most of the reversed incident field (black arrow), leading to a high directional emission exactly around the WS₂ emission band ($\lambda = 633$ nm), as shown in Fig. 4(f). It is noted that the reversed incident field is not completely canceled out, as manifested by the phase arrows that are not fully looped, which accounts for the tiny side lobes in the backward direction. The above analysis strongly suggests that the self-hybridized nanowire system can serve as an efficient nanoantenna to modulate light emission in a desired way, thus providing a promising platform for realizing novel quantum light emitters with high compatibility.

III. CONCLUSIONS

In conclusion, we proposed a nanowire composed of bulk WS₂ to explore the self-hybridization under the excitation of the electric dipole source, demonstrating the flexible tuning of light emission directionality. We demonstrated the exciton-Mie self-hybridization in strong coupling regime with a large coupling energy over 120 meV. The influence of the oscillator strength on the directional emission property was studied by “switching on/off” the intrinsic excitonic resonance. We reveal that the emission directionality can be effectively modulated by the exciton-Mie self-hybridization in the nanowire, leading to a dramatic suppression of directional emission at the excitonic resonance. In addition, we realized unidirectional and directional emission for monolayer WS₂ by choosing a suitable nanowire radius. Two mechanisms are explained with the help of multipole expansion and phase-representation diagrams. Our work supports more possibilities for the design of quantum light emitters and provides a new route for improving the efficiency of optoelectronic systems with new functions, which is conducive to the design and realization of novel optical quantum devices, ranging from solid-state lighting and displays to nanoscale single-photon sources.

ACKNOWLEDGMENTS

This work was supported by the National Natural Science Foundation of China (Grants No. 11974254 and No. 11974253), and Science Specialty Program of Sichuan University (Grant No. 2020SCUNL210).

- [1] Y. H. Fu, A. I. Kuznetsov, A. E. Miroshnichenko, Y. F. Yu, and B. Luk'yanchuk, *Nat. Commun.* **4**, 1527 (2013).
- [2] Y. W. Xie, S. H. Hong, H. Yan, C. P. Zhang, L. Zhang, L. M. Zhuang, and D. X. Dai, *Opto-Electron. Adv.* **6**, 220030 (2023).
- [3] Y. L. Wang, C. J. Min, Y. Q. Zhang, and X. C. Yuan, *Opto-Electron. Adv.* **5**, 210047 (2022).
- [4] P. Muhlschlegel, H. J. Eisler, O. J. F. Martin, B. Hecht, and D. W. Pohl, *Science* **308**, 1607 (2005).
- [5] K. F. Mak and J. Shan, *Nat. Photonics* **10**, 216 (2016).
- [6] A. J. Shields, *Nat. Photonics* **1**, 215 (2007).

- [7] A. S. Sharbirin, S. Akhtar, and J. Kim, *Opto-Electron. Adv.* **4**, 200077 (2021).
- [8] C. Bradac, W. Gao, J. Forneris, M. E. Trusheim, and I. Aharonovich, *Nat. Commun.* **10**, 5625 (2019).
- [9] P. Cheben, R. Halir, J. H. Schmid, H. A. Atwater, and D. R. Smith, *Nature (London)* **560**, 565 (2018).
- [10] W. Choi, N. Choudhary, G. H. Han, J. Park, D. Akinwande, and Y. H. Lee, *Mater. Today* **20**, 116 (2017).
- [11] J. Fang, M. Wang, K. Yao, T. Zhang, A. Krasnok, T. Jiang, J. Choi, E. Kahn, B. A. Korgel, M. Terrones, X. Li, A. Alu, and Y. Zheng, *Adv. Mater.* **33**, 2007236 (2021).

- [12] D. G. Baranov, R. S. Savelev, S. V. Li, A. E. Krasnok, and A. Alù, *Laser Photonics Rev.* **11**, 1600268 (2017).
- [13] L. Novotny and N. van Hulst, *Nat. Photonics* **5**, 83 (2011).
- [14] A. I. Kuznetsov, A. E. Miroshnichenko, M. L. Brongersma, Y. S. Kivshar, and B. Luk'yanchuk, *Science* **354**, 2472 (2016).
- [15] T. Kosako, Y. Kadoya, and H. F. Hofmann, *Nat. Photonics* **4**, 312 (2010).
- [16] T. Shegai, S. Chen, V. D. Miljkovic, G. Zengin, P. Johansson, and M. Kall, *Nat. Commun.* **2**, 481 (2011).
- [17] E. M. You, Y. Q. Chen, J. Yi, Z. D. Meng, Q. Chen, S. Y. Ding, H. G. Duan, M. Moskovits, and Z. Q. Tian, *Opto-Electron. Adv.* **4**, 210076 (2021).
- [18] D. Vercruyse, Y. Sonnefraud, N. Verellen, F. B. Fuchs, G. Di Martino, L. Lagae, V. V. Moshchalkov, S. A. Maier, and P. Van Dorpe, *Nano Lett.* **13**, 3843 (2013).
- [19] G. V. Naik, V. M. Shalaev, and A. Boltasseva, *Adv. Mater.* **25**, 3264 (2013).
- [20] J. B. Khurgin, *Nat. Nanotechnol.* **10**, 2 (2015).
- [21] J. A. Schuller, R. Zia, T. Taubner, and M. L. Brongersma, *Phys. Rev. Lett.* **99**, 107401 (2007).
- [22] P. Spinelli, M. A. Verschuuren, and A. Polman, *Nat. Commun.* **3**, 692 (2012).
- [23] I. Staude, V. V. Khardikov, N. T. Fofang, S. Liu, M. Decker, D. N. Neshev, T. S. Luk, I. Brener, and Y. S. Kivshar, *ACS Photonics* **2**, 172 (2015).
- [24] L. Y. Cao, J. S. White, J. S. Park, J. A. Schuller, B. M. Clemens, and M. L. Brongersma, *Nat. Mater.* **8**, 643 (2009).
- [25] Q. R. Deng, J. F. Chen, L. Long, B. Q. Chen, H. K. Yu, and Z. Y. Li, *Opto-Electron. Adv.* **5**, 210024 (2022).
- [26] M. L. Brongersma, Y. Cui, and S. Fan, *Nat. Mater.* **13**, 451 (2014).
- [27] R. M. Bakker, D. Permyakov, Y. F. Yu, D. Markovich, R. Paniagua-Dominguez, L. Gonzaga, A. Samusev, Y. Kivshar, B. Luk'yanchuk, and A. I. Kuznetsov, *Nano Lett.* **15**, 2137 (2015).
- [28] J. Cambiasso, G. Grinblat, Y. Li, A. Rakovich, E. Cortes, and S. A. Maier, *Nano Lett.* **17**, 1219 (2017).
- [29] A. B. Evlyukhin, C. Reinhardt, A. Seidel, B. S. Luk'yanchuk, and B. N. Chichkov, *Phys. Rev. B* **82**, 045404 (2010).
- [30] A. García Etxarri, R. Gómez-Medina, L. S. Froufe-Pérez, C. López, L. Chantada, F. Scheffold, J. Aizpurua, M. Nieto-Vesperinas, and J. J. Sáenz, *Opt. Express* **19**, 4815 (2011).
- [31] R. Paniagua Domnguez, Y. F. Yu, A. E. Miroshnichenko, L. A. Krivitsky, Y. H. Fu, V. Valuckas, L. Gonzaga, Y. T. Toh, A. Y. S. Kay, B. Luk'yanchuk, and A. I. Kuznetsov, *Nat. Commun.* **7**, 10362 (2016).
- [32] I. Staude, A. E. Miroshnichenko, M. Decker, N. T. Fofang, S. Liu, E. Gonzales, J. Dominguez, T. S. Luk, D. N. Neshev, I. Brener, and Y. Kivshar, *ACS Nano* **7**, 7824 (2013).
- [33] S. Person, M. Jain, Z. Lapin, J. J. Sáenz, G. Wicks, and L. Novotny, *Nano Lett.* **13**, 1806 (2013).
- [34] J. Li, N. Verellen, D. Vercruyse, T. Bearda, L. Lagae, and P. Van Dorpe, *Nano Lett.* **16**, 4396 (2016).
- [35] Y. Yu, J. Z. Liu, Y. D. Yu, D. Y. Qiao, Y. Q. Li, and R. Salas-Montiel, *Opt. Express* **30**, 7918 (2022).
- [36] S. Busschaert, R. Reimann, M. Cavigelli, R. Khelifa, A. Jain, and L. Novotny, *ACS Photonics* **7**, 2482 (2020).
- [37] R. Verre, D. G. Baranov, B. Munkhbat, J. Cuadra, M. Kall, and T. Shegai, *Nat. Nanotechnol.* **14**, 679 (2019).
- [38] N. Muhammad, Y. Chen, C.-W. Qiu, and G. P. Wang, *Nano Lett.* **21**, 967 (2021).
- [39] T. Weber, L. Kühner, L. Sortino, A. Ben Mhenni, N. P. Wilson, J. Kühne, J. J. Finley, S. A. Maier, and A. Tittl, *Nat. Mater.* **22**, 970 (2023).
- [40] A. Canales, O. Kotov, and T. O. Shegai, *ACS Nano* **17**, 3401 (2023).
- [41] P. Xie, Q. Ding, Z. C. Liang, S. Y. Shen, L. Yue, H. Zhang, and W. Wang, *Phys. Rev. B* **107**, 075415 (2023).
- [42] A. F. Cihan, A. G. Curto, S. Raza, P. G. Kik, and M. L. Brongersma, *Nat. Photonics* **12**, 284 (2018).
- [43] B. Munkhbat, D. G. Baranov, M. Stuhrenberg, M. Wersall, A. Bisht, and T. Shegai, *ACS Photonics* **6**, 139 (2019).
- [44] S. Y. Shen, Y. Y. Wu, Y. H. Li, P. Xie, Q. Ding, X. Y. Kuang, W. X. Wang, and W. Wang, *Phys. Rev. B* **105**, 155403 (2022).
- [45] P. Xie, Y. H. Deng, L. X. Zeng, Z. C. Liang, S. Y. Shen, Q. Ding, H. Zhang, Z. K. Zhou, and W. Wang, *Phys. Rev. B* **106**, 165408 (2022).
- [46] P. Xie and Y. Cheng, *Phys. Rev. B* **108**, 155412 (2023).